ELSEVIER

Polymer 40 (1999) 6475–6484

polymer

Crystallization of oriented amorphous poly(ethylene terephthalate) as revealed by X-ray diffraction and microhardness

Tsutomu Asano[a,*], Francisco J. Baltá Calleja[b], Araceli Flores[b], Motonori Tanigaki[a], Mohammad Forhad Mina[a], Chie Sawatari[c], Hideyuki Itagaki[c], Hiroshi Takahashi[d], Ichiro Hatta[d]

[a]*Department of Physics, Faculty of Science, Shizuoka University, Shizuoka 422-8529, Japan*
[b]*Instituto de Estructura de la Materia, C.S.I.C., Serrano 119, 28006 Madrid, Spain*
[c]*Faculty of Education, Shizuoka University, Shizuoka 422-8529, Japan*
[d]*Department of Applied Physics, Graduate School of Engineering, Nagoya University, Nagoya 464-8603, Japan*

Received 26 June 1998; received in revised form 26 October 1998; accepted 1 December 1998

Abstract

The structural changes occurring when amorphous cold-drawn poly(ethylene terephthalate) films are annealed at different temperatures (50°C–240°C) for different annealing times (10–10^4 s) were investigated by means of X-ray diffraction and microhardness techniques. The X-ray results reveal the appearance of smectic order at 60°C with a period of 10.7 Å. At 70°C, a layer structure in the scale of 110 Å emerges. Finally, triclinic order is observed above 80°C. The appearance of a layer structure prior to the development of triclinic crystals is associated with a density difference along the molecular direction produced by a molecular tilting mechanism. The microhardness behaviour of annealed cold-drawn PET films is correlated to the developing morphologies. At high annealing temperatures (>100°C), the plastic component of hardness is shown to vary with the occurring microstructural changes. Results indicate that the hardness of the amorphous intrafibrilar regions is higher than that of a fully amorphous material. The indentation anisotropy, ΔH, which is related to the elastic recovery of the material shows a conspicuous decrease at $T_a \backsim 70$°C, which is explained in terms of a relaxation of the fibrils in the chain direction.

Keywords: Poly(ethylene terephthalate); X-ray diffraction; Microhardness

1. Introduction

It is well known that poly(ethylene terephthalate) (PET) solidifies in the form of an amorphous glass when quenched from the melt [1,2]. Morphological studies of primary crystallization in PET were performed by several authors [3–6]. When drawing above the glass transition temperature (T_g), Bonart was the first to report the occurrence of a paracrystalline structure [7]. This author observed that the structure of PET varied during the drawing treatment from a totally amorphous to a nematic and finally to a smectic state. From electron microscopic observations, Yeh and Geil pointed out that glassy PET is composed of ball-like structures in which molecules exhibit a paracrystalline order [8,9]. According to these authors, strain-induced crystallization can be explained by rotation, alignment and perfection of the internal order of the paracrystalline ball-like structure.

Triclinic PET sometimes reveals a unique tilted orientation (the 230 orientation), which was first studied by Daubeny et al. [10]. Asano and Seto later analysed, in detail, the dependence of the molecular tilted orientation on the annealing temperature. These authors proposed a monoclinic paracrystalline structure in the early stages of crystallization from an oriented glass [11] which enables to explain the variation of the tilted orientation.

Microindentation studies on a wide variety of polymeric materials provide experimental evidence of a close relationship between microhardness and several microstructural parameters such as crystalline lamellar thickness, crystallinity, polymorphism, etc. [12–14]. Microhardness, H, of isotropic PET was extensively studied [15–18]. Recently, the mechanical anisotropy of injection moulded PET was measured [19].

In the present article, we report new morphological studies of cold-drawn PET as revealed by X-ray diffraction and hardness measurements. The mechanism of crystallization of oriented glassy PET, especially in the initial stages of crystallization below 100°C, is discussed. The correlation

* Corresponding author. Tel.: + 81-54-238-4743; fax: + 81-54-238-4743.
E-mail address: sptasan@sci.shizuoka.ac.jp (T. Asano)

0032-3861/99/$ - see front matter © 1999 Elsevier Science Ltd. All rights reserved.
PII: S0032-3861(98)00839-8

between the structure developed during crystallization of drawn PET and the corresponding mechanical properties is highlighted.

2. Experimental

2.1. Cold drawing and annealing treatments

Amorphous PET was synthesized by Toray Co. Ltd. Japan ($M_n = 18\,000$). The isotropic sample film (thickness ~0.5 mm) was drawn at room temperature using a Tensilon UTM 4-100, Toyo Boldwin Co. Ltd. The drawing speed and the average draw ratio were 0.8 mm/min and 3.8, respectively. The film was slightly whitened by the uniaxial drawing, with a final thickness of 0.15 mm.

The annealing treatment of the cold-drawn PET samples was performed with fixed ends maintaining the length of the sample constant. Samples annealed at temperatures, T_a, lower than 160°C were immersed in a silicone oil bath. The temperature was controlled with an accuracy of ±0.1°C. The annealing times, t_a, used for each annealing temperature were 10, 10^2 and 10^3 s. An oven was used to anneal the samples above 160°C. Owing to the low heat conductivity of the air oven, only long annealing times were used. Hence, samples annealed at temperatures in the range 50°C–240°C for 10^4 s were prepared.

2.2. X-ray diffraction measurements

Wide angle (WAXS), middle angle (MAXS) and small angle (SAXS) X-ray scattering patterns of the annealed samples were obtained. MAXS experiments were carried out in order to record simultaneously the WAXS and SAXS diffraction maxima in one photograph ($2\theta \sim 1°$–$10°$).

WAXS and SAXS patterns of the annealed samples were taken at room temperature using a Rigaku 4012A and RU300 generator, respectively, with a wavelength of 1.54 Å. The camera length and exposure time were 5 cm and 1 h for the WAXS experimental and 26 cm and 3 h for the SAXS measurements, respectively. The WAXS patterns recorded correspond to the samples annealed at $T_a \leq 100$°C ($t_a = 10$–10^4 s). SAXS experiments were carried out on samples annealed at $T_a \geq 100$°C for $t_a = 10^4$ s.

In-situ MAXS measurements were performed at Photon Factory, National Laboratory for High Energy Physics, Tsukuba, Japan, using a vacuum path with a camera length of 86 cm. The oriented amorphous sample was sandwiched between two metal rings of 7 mm diameter to prevent shrinkage during heating. The metal rings were then placed in the Mettler FP-99 heating facility [20]. The sample was heated at 10°C/min up to T_a ($T_a \leq 100$°C) and held thereafter for 60 s. The exposure time for one MAXS pattern photographed by Imaging Plate (IP) of Fuji Film Co. Ltd. was 60 s. The wavelength used was 1.506 Å.

2.3. Density

The density, ρ, of the drawn PET samples annealed at different temperatures for 10^4 s was measured by the floating method using a Lipkin's pycnometer, with *n*-heptane and carbon tetrachloride as a medium.

2.4. Degree of crystallinity

The volume degree of crystallinity, α_c, of the investigated PET samples was derived from density as follows:

$$\alpha_c = (\rho - \rho_a)/(\rho_c - \rho_a), \tag{1}$$

where ρ_a and ρ_c are the densities of the amorphous and crystalline phases respectively. The amorphous density of PET is taken to be $\rho_a = 1.37$ g/cm^3, which is the measured density of the amorphous cold-drawn sample without further annealing (mentioned later). The density of the triclinic crystalline phase of PET is taken to be $\rho_c = 1.455$ g/cm^3 [10].

2.5. Microhardness

Microindentation experiments were carried out at room temperature (~21°C). A Vickers square-based diamond pyramid (included angle of 136° between opposite faces) was used. Vickers hardness is calculated as follows:

$$H = k\frac{P}{d^2}, \tag{2}$$

where P is the load applied, d the measured diagonal of the residual impression and k is a geometric constant. A value of $k = 1.854$ is used when P is in N and d in mm to give H in MPa. The load applied was of 980 mN, which was held for 6 s to minimize the creep of the sample under the indenter [12]. The P/d^2 ratio was observed to be constant for different loads, i.e. the elastic recovery was negligible [21]. The accuracy in the indentation diagonal was of ±1.2 μm. Owing to sample orientation, the residual impression shows anisometric diagonal lengths. We define $H_{\parallel}$ as the hardness derived from the measurement of the indentation diagonal parallel to the drawing direction and $H_{\perp}$ as the value derived from the diagonal length perpendicular to the drawing direction. The indentation anisotropy, ΔH, is calculated following [12]:

$$\Delta H = 1 - \frac{H_{\perp}}{H_{\parallel}}. \tag{3}$$

2.6. Mechanical models

The hardness of a polymeric material, H, is well described by a parallel model of alternating amorphous and crystalline regions, with hardness values H_a and H_c respectively, following [13]:

$$H = H_c\alpha_c + H_a(1 - \alpha_c), \tag{4}$$

where α_c is the volume degree of crystallinity. H_c is related

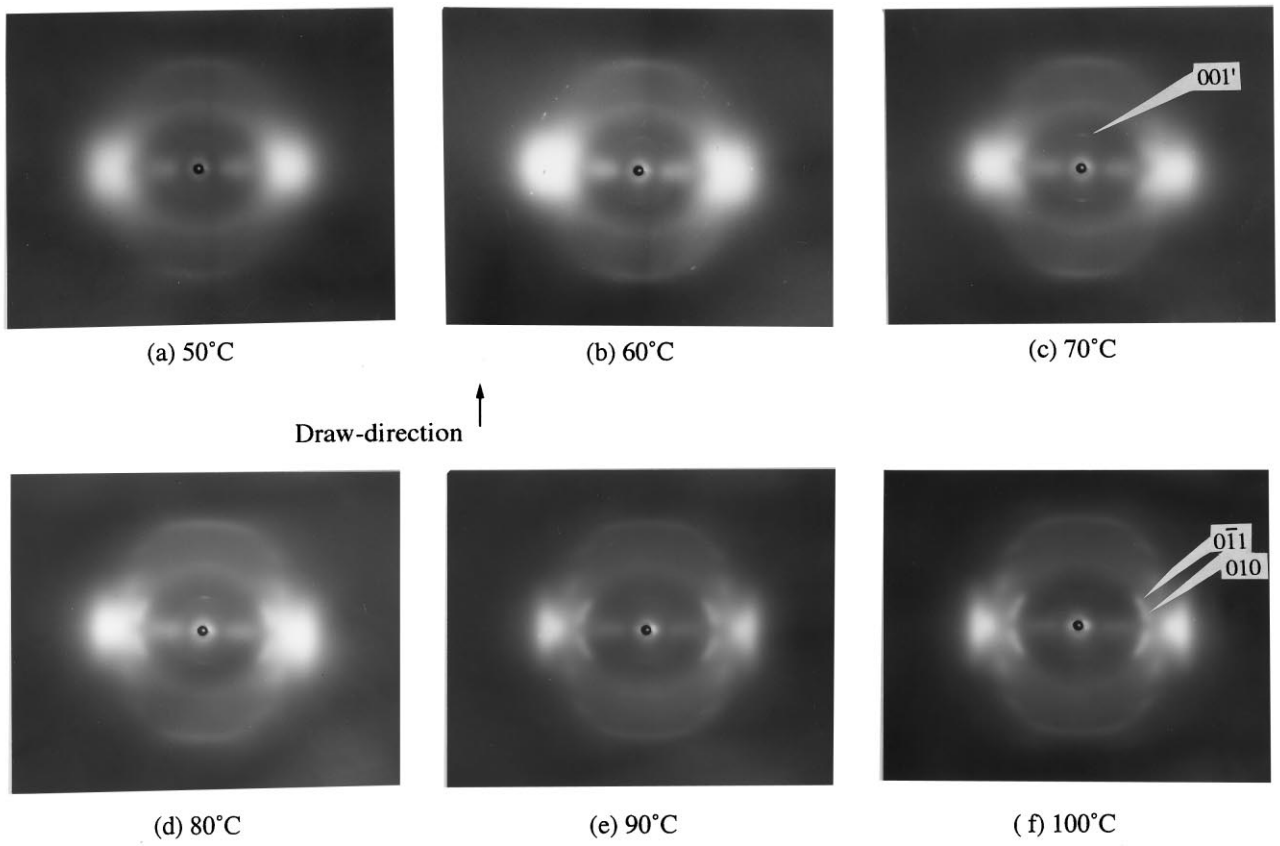

Fig. 1. WAXS patterns of cold-drawn PET taken at room temperature after annealing during 10 s at a temperature of: (a) 50°C, (b) 60°C, (c) 70°C, (d) 80°C, (e) 90°C and (f) 100°C.

to the crystalline lamellar thickness, l_c, through [13]:

$$H_c = \frac{H_c^{\infty}}{1 + (b/l_c)}, \quad (5)$$

where H_c^{∞} is the hardness of an infinitely thick crystal and $b = 2\sigma_e/\Delta h$ is a parameter related to the surface free energy σ_e of the crystals and to the energy Δh required for plastic deformation of the latter.

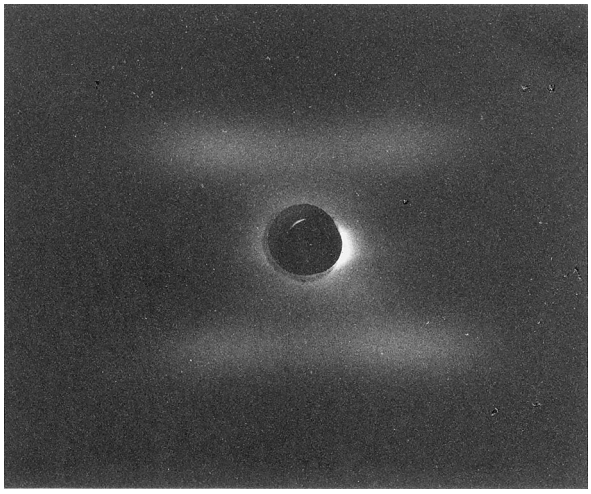

Fig. 2. SAXS diagram of the PET film annealed at 200°C for $t_a = 10^4$ s.

3. Results

3.1. Measurements at room temperature

3.1.1. Wide angle X-ray scattering

The WAXS patterns of cold-drawn PET annealed at different temperatures ($t_a = 10$ s) are presented in Fig. 1. X-ray diffraction of the original cold-drawn sample has a broad maximum centred on the equator. The scattering pattern does not change upon annealing at 50°C for 10 s (Fig. 1a). The occurrence of a diffuse equatorial diffraction maximum indicates that PET molecules are preferentially aligned parallel to the draw direction with absence of crystalline order.

In Fig. 1b–d, a weak but sharp reflection appears on the meridian. The spacing of this reflection is measured as 10.7 Å. We index this reflection as $001'$ as the spacing nearly corresponds to the monomer length (10.75 Å) of PET. The $001'$ reflection also appears when the amorphous sample is annealed at 50°C for 10^2 s. The intensity of the $001'$ reflection changes in the temperature range of 60°C–80°C, depending on T_a and t_a. The highest intensity of $001'$ for $t_a = 10$ s is observed at $T_a = 70$°C, as shown in Fig. 1c. The equatorial maximum is still rather broad below 70°C indicating that the oriented PET molecules have no lateral crystalline order. For $T_a > 80$°C, the intensity of the $001'$

Table 1
Long period in the drawing direction, lamellar inclination angle, degree of crystallinity and crystalline lamellar thickness for PET annealed at a temperature T_a ($t_a = 10^4$ s)

T_a (°C)	L (Å)	ϕ (°)	α_c	l_c (Å)
100	110	55	0.22	14
120	111	50	0.28	20
140	113	46	0.35	28
160	117	44	0.41	35
180	120	41	0.48	44
200	124	40	0.55	52
220	140	38	0.63	70
240	158	37	0.72	91

reflection clearly decreases. Simultaneously, the triclinic 010 and $0\bar{1}1$ reflections become distinct from the equatorial diffuse peak. At $T_a = 90$°C, the meridional $001'$ reflection almost disappears and the equatorial triclinic 010 reflection increases in intensity (see Fig. 1e). At $T_a = 100$°C, the triclinic 010 reflections are displaced up and down from the equator, indicating that the triclinic (010) plane is inclined by 10° from the draw direction (see Fig. 1f).

3.1.2. Small angle X-ray scattering

SAXS measurements on samples annealed at $T_a \geq 100$°C for $t_a = 10^4$ s yield four-point patterns (see Fig. 2 for $T_a =$ 220°C). From the four-point patterns recorded, we can evaluate the lameller spacing, L, along the drawing direction and the lamellar inclination angle, ϕ, between the normal to the lamellar and the drawing direction. The values of L and ϕ for different T_a are listed in Table 1.

3.1.3. Density

Fig. 3 illustrates the plot of the density of the drawn samples vs. T_a ($t_a = 10^4$ s). The density of the oriented glassy PET sample ($T_a = 20$°C) is 1.37 g/cm^3, i.e., higher than the value of isotropic amorphous PET (1.335 g/cm^3) [10]. The density values show a monotonous increase with

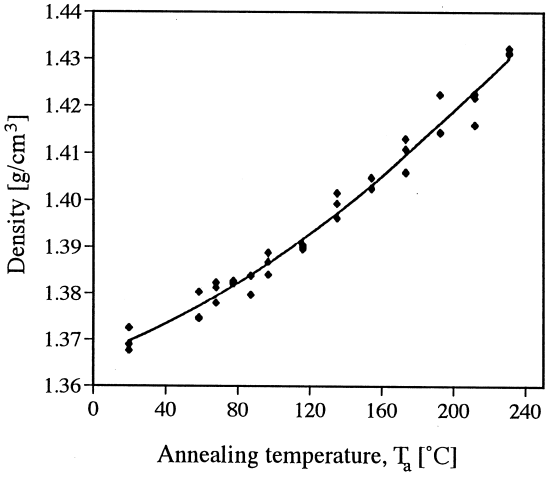

Fig. 3. Density variation with annealing temperature ($t_a = 10^4$ s).

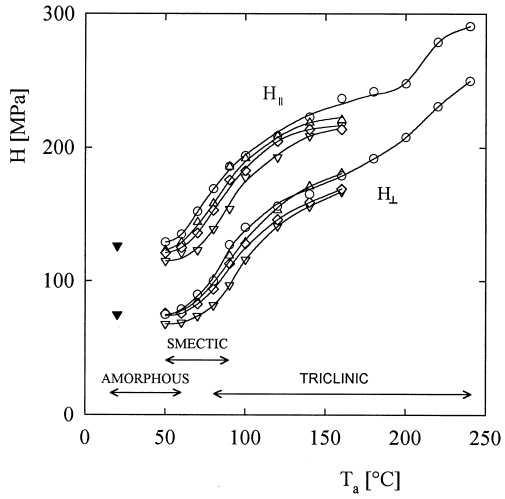

Fig. 4. $H_{\parallel}$ and $H_{\perp}$ as a function of the annealing temperature for different annealing times: ▽: $t_a = 10$ s; ◇: $t_a = 10^2$ s; △: $t_a = 10^3$ s; ○: $t_a = 10^4$ s; ▼: cold-drawn sample without further annealing.

T_a. The crystalline lamellar thickness along the axis normal to the lamella, l_c, was evaluated from:

$$l_c = \alpha_c L \cos \phi, \tag{6}$$

where α_c is derived from density measurements using Eq. (1). The values of α_c and l_c for $T_a \geq 100$°C are also listed in Table 1.

3.1.4. Microhardness

Fig. 4 shows $H_{\parallel}$ and $H_{\perp}$ values as a function of the annealing temperature for different annealing times. The hardness value for the cold-drawn sample before annealing ($T_a =$ 20°C) has also been included. $H_{\perp}$ values are related to the plastic deformation mode of the lamellar stacks within the fibrous oriented structure. The higher $H_{\parallel}$ values with respect

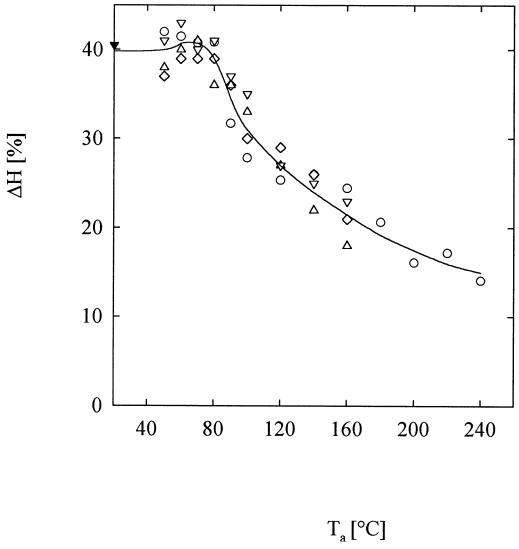

Fig. 5. ΔH as a function of the annealing temperature for different annealing times. Symbols as in Fig. 4.

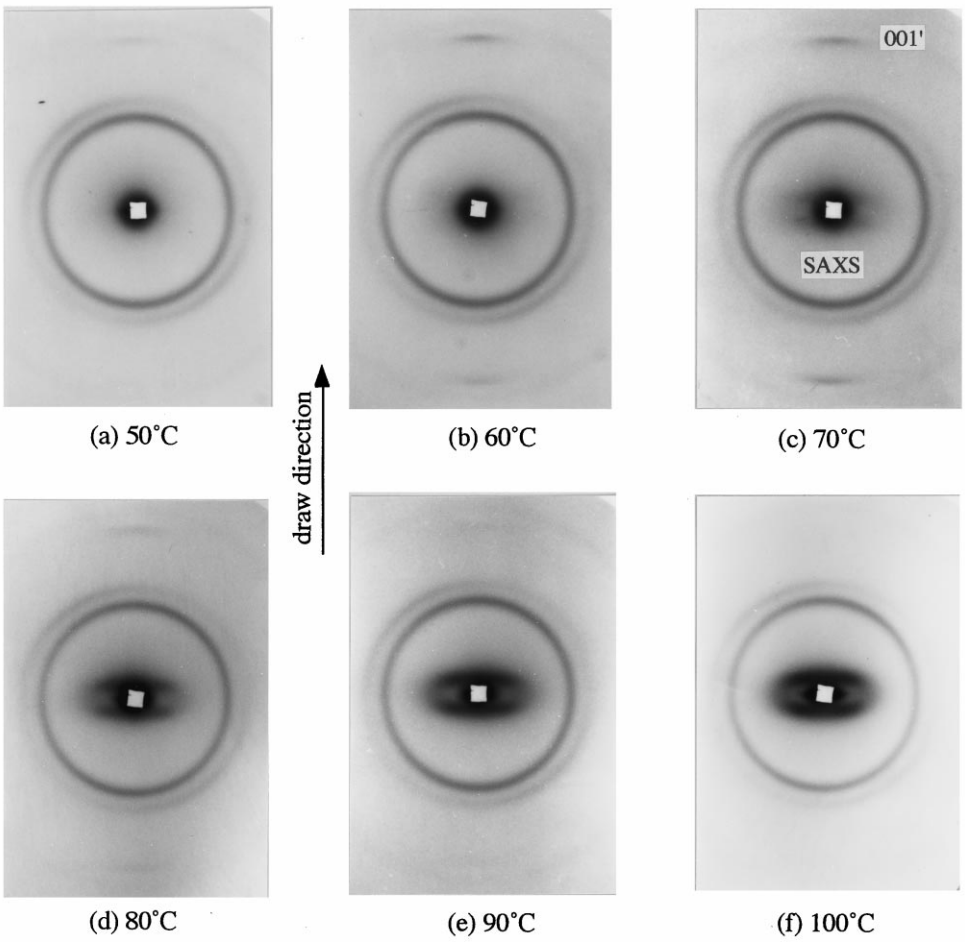

Fig. 6. In-situ MAXS patterns obtained at different annealing temperatures: (a) 50°C, (b) 60°C, (c) 70°C, (d) 80°C, (e) 90°C, (f) 100°C.

to the $H_{\perp}$ values for the four series of annealed PET samples (t_a = 10, 10^2, 10^3 and 10^4 s) are a consequence of the instant elastic recovery of the fibrils after removal of the indenter and therefore contribute to the smaller indentation dimension.

Fig. 5 illustrates the variation of the indentation anisotropy as a function of T_a for the series of PET samples annealed at different t_a. Anisotropy ΔH is a measure of the elastic recovery of the material and was correlated to the longitudinal elastic modulus in other oriented polymer samples [12,22]. The first finding in Fig. 5 is the unusual high ΔH values found for the samples investigated. At the lowest annealing temperatures ($T_a < 70$°C), $\Delta H \sim 40\%$, which is a large indentation anisotropy value as compared to that reported on injection moulded PET [19] where the maximum ΔH achieved was of 15%. Most interesting is the fact that above $T_a \sim 70$°C, which is a temperature close to the glass transition temperature (T_g) of PET, ΔH decreases rapidly with T_a.

3.2. In-situ MAXS measurements

The results of the MAXS experiments are shown in Fig. 6. The isotropic rings in the MAXS patterns are artifacts originated from the polymer film placed in the vacuum path. The meridional $001'$ reflection is located out of the isotropic ring as indicated in Fig. 6c. The SAXS reflection appears near the centre of the pattern at temperatures 70°C and above (Fig. 6c–f). The spacing of the SAXS reflection is approximately constant over the range of T_a considered and equal to 110 Å. Hence, the lamella along the drawing direction comprises roughly 10 monomer units. The inclination angle ϕ at T_a = 70°C is $\sim 62°$. As the annealing temperature increases, the meridional reflection progressively weakens while the SAXS reflection increases in intensity. At T_a = 100°C, the meridional $001'$ reflection completely disappears.

4. Discussion

4.1. Crystallization process

In order to summarize the various steps of the crystallization process from the glass, the results of the WAXS, MAXS and SAXS measurements are schematically

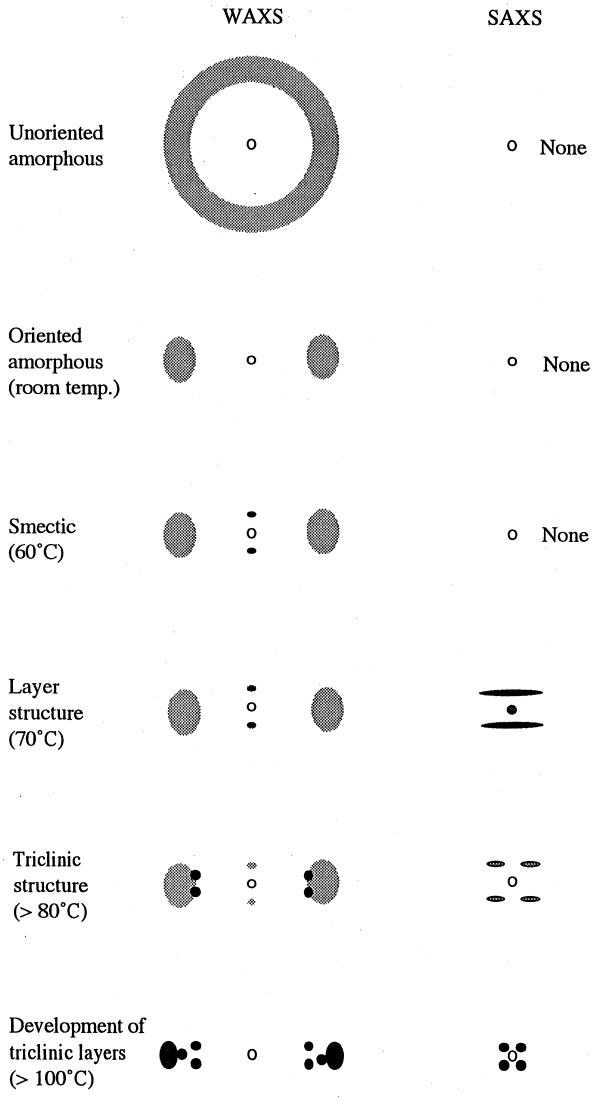

Fig. 7. Summary of the X-ray results during the crystallization.

illustrated in Fig. 7. The intensity of the meridional, the SAXS and the triclinic reflections at different temperatures are compared in Table 2.

4.1.1. Molecular orientation by cold drawing

Cold drawing of glassy PET at room temperature through necking induces preferential alignment of the chain axis along the draw direction. Some molecular segments could be randomly oriented or partly entangled owing to the limited mobility at temperatures well below T_g. However, considering the applied draw ratio of 3.8 and the high density achieved (1.37 g/cm^3), one must conclude that a significant number of molecules are aligned nearly parallel to the draw direction. The orientational order exhibited could be described by a nematic state as schematically depicted in Fig. 8a. The circles in the molecular chains represent benzene rings separated by 10.75 Å intervals. The lateral position of each benzene ring deviates with respect to the neighbouring molecules.

Table 2
Observation of 001′, triclinic reflections in WAXS and layer structures in SAXS. ×: disappearance △: weak appearance ○: appearance

T_a (°C)	001′ (WAXS)	Triclinic (WAXS)	Layer (SAXS)
Room temp.	×	×	×
50	△	×	×
60	○	×	×
70	○	×	△
80	○	△	○
90	△	○	○
100	×	○	○

4.1.2. Analysis of the meridional reflection

The meridional reflection is first apparent at $T_a = 50$°C–60°C (depending on t_a). The spacing is almost equal to the monomer unit length. This result suggests that neighbouring molecular segments laterally tend to match at temperatures below T_g.

Fig. 8b schematically shows the occurrence of the smectic phase developed from the nematic state. The benzene rings of the smectic state are arranged on planes perpendicular to the draw direction, whereas the lateral packing of the neighbouring molecules has no crystalline order. The smectic state is presumably attained through an increase in the mobility of the molecular segments leading to a slightly higher densely packed structure ($\rho = 1.38$ g/cm^3) than that of the nematic one.

4.1.3. Development of the lamellar structure

The appearance of a diffuse SAXS reflection at $T_a = 70$°C prior to the development of the triclinic crystal is most interesting. The result suggests the existence of a precursor state before the triclinic state. Considering that here T_a is on the vicinity of T_g, molecular motions are insufficient so as to form a large-scale structure giving the SAXS reflection. Hence, we propose a molecular tilting mechanism in the smectic phase which implies a minimum cooperative displacement. This tilting mechanism could produce a density difference within the smectic structure and hence could explain the structure observed in SAXS. The precursor state at $T_a = 70$°C is schematically illustrated in Fig. 9.

4.1.4. Tilting mechanism

One possibility to explain the periodic density difference observed along the molecular direction at $T_a = 70$°C could be in terms of a combination of a molecular tilt mechanism and the inclination of the layer surface. To estimate the density difference along the molecular direction, we first calculate the average lateral distance between molecules in the smectic state. The volume of the triclinic unit cell, V_c, from Ref. [10] is 218.95 Å^3. The average smectic volume, V_{sm}, is estimated as follows:

$$V_{sm} = (\rho_c/\rho_{sm})V_c = 230.85\ \text{Å}^3, \quad (7)$$

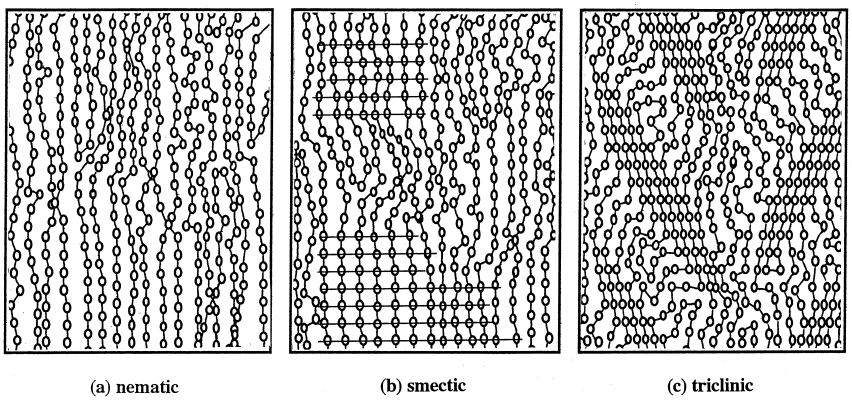

Fig. 8. Schematic representation of the morphological changes: (a) nematic phase, (b) smectic phase and (c) triclinic structure.

where $\rho_c = 1.455$ g/cm^3 [10] and $\rho_{sm} = 1.38$ g/cm^3 is the smectic density observed at 70°C (see Fig. 3). The average molecular cross section is derived as 230.85 Å^3/10.75 Å = 21.47 Å^2 and the average molecular distance is calculated as 5.23 Å (see Fig. 9a).

If we assume that the lamellar surface fits to the shift of one monomer unit (see Fig. 9a), then the inclination angle ϕ of the lamella is calculated as:

$$\phi = \tan^{-1}(10.75/5.23) = 64°. \quad (8)$$

This value is consistent with the value (~62°) obtained from the MAXS pattern at 70°C.

Assuming that the tilt of the smectic molecules alternates by an angle $\pm\delta$ from the draw direction, the inclined layer produces a packing difference between regions A and C (Fig. 9a). The ratio between the densities in the A and C regions can be calculated from the ratio between the lateral dimensions in A and C, d_A/d_C. For a value of $\delta = 1°$:

$$d_A/d_C = \sin(90° - 64° + \delta)/\sin(90° - 64° - \delta) = 1.074. \quad (9)$$

However, the quotient between the amorphous and the triclinic density is equal to:

$$\rho_c/\rho_a = 1.455/1.37 = 1.062. \quad (10)$$

Thus the estimated d_A/d_C ratio in the precursor state seems to be sufficient to produce the required electron density contrast. Moreover, using $\delta = 1°$ and $L = 110$ Å, the maximum lateral deviation, Δx, from the draw direction is calculated to be less than 1 Å (Fig. 9b). The small δ and Δx values are likely to occur in the initial stages of crystallization at temperatures in the vicinity of T_g.

The aforementioned discussion strongly suggests that a tilting mechanism could produce the precursor state at 70°C.

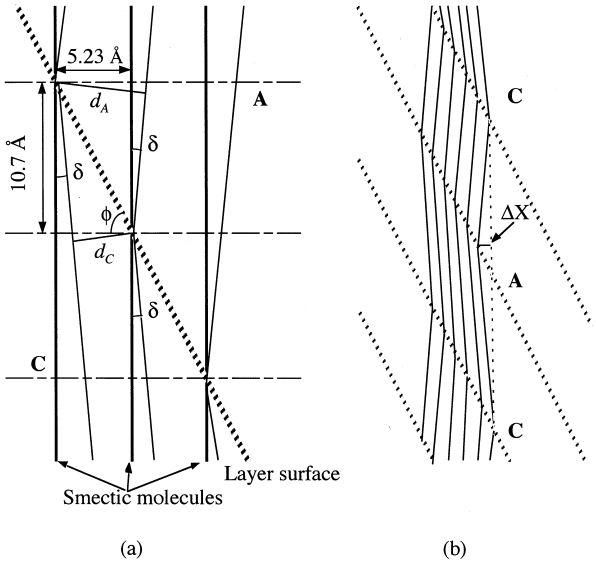

Fig. 9. The tilting mechanism occurring in the precursor state: (a) The density difference between A and C regions. (b) The molecular displacement in the precursor state.

4.1.5. Development of triclinic crystals

The WAXS results in Fig. 1 indicate that the triclinic crystal develops above 80°C. In the preceding section, we suggest that the precursor state is formed by a slight tilt of the smectic molecules. The triclinic structure is then developed at $T_a > 80$°C by a further tilt of the molecules within the crystalline lamellae. As shown in the WAXS patterns of Fig. 1f, the triclinic (010) plane is 10° inclined from the draw direction. Considering the triclinic crystal structure with the crystallographic angle $\alpha = 98.5°$ [10], the crystalline *b*-axis is nearly perpendicular to the draw direction. This fact strongly supports the concept that the normal to the benzene rings' planes is maintained parallel to the draw direction during the initial crystallization process from the smectic structure through the precursor state into the triclinic phase. Fig. 8c schematically shows the development of the triclinic crystals at 100°C with the *b*-axis nearly perpendicular to the draw direction.

Further annealing at higher temperatures thickens the crystalline lamellae as shown in Table 1. Entanglements and folds will concentrate especially at high T_a, in the amorphous lamellae.

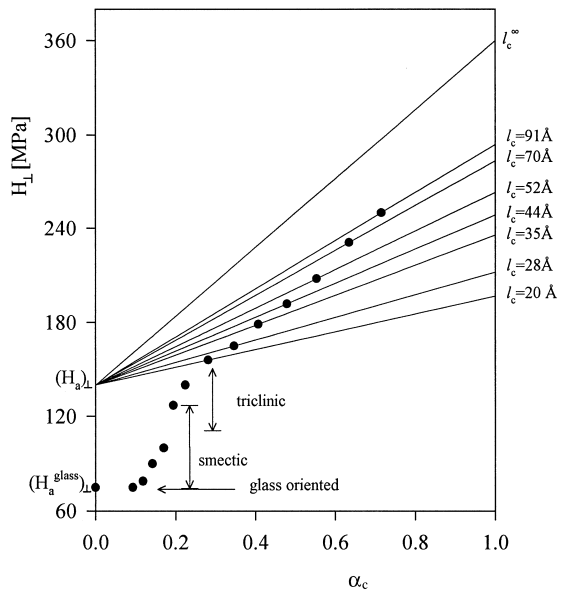

Fig. 10. $H_\perp$ variation with α for the samples annealed during 10^4 s. The straight lines follow Eq. (4), with $(H_a)_\perp = 140$ MPa.

4.2. Mechanical properties: microhardness

4.2.1. Influence of annealing temperature

In Fig. 4, one can distinguish four regions of $H_\perp$ behaviour which correlate to the various structures appearing when T_a is increased.

1. $T_a \leq 60$°C: WAXS diagrams reveal the existence of an amorphous oriented phase at room temperature and the emerging of a smectic order at $T_a = 50$°C–60°C (Fig. 1b). These structural changes occurring below 60°C do not seem to influence substantially the $H_\perp$ values.
2. 60°C $< T_a \leq$ 80°C: In this temperature range, $H_\perp$ slightly varies with T_a. Here the smectic phase is the main structure appearing. At $T_a = 70$°C, the amount of smectic domains present is sufficient to produce an appreciable $H_\perp$ increase. In addition, a layer structure emerges at $T_a = 70$°C as revealed by MAXS (Fig. 6c).
3. 80°C $< T_a <$ 100°C: The $H_\perp$ increase observed above 70°C can be considered as owing to an enhancement of molecular motion facilitated beyond T_g. The step $H_\perp$ variation with T_a from $T_a = 80$°C up to $T_a \sim 100$°C is associated with the developing of a triclinic structure while the smectic domains start to disappear.
4. $T_a \geq 100$°C: At $T_a = 100$°C, the smectic phase completely disappears and a three-dimensional crystalline order develops as revealed by WAXS (Fig. 1). Contrary to what was observed for isotropic PET [15], there is a further hardness increase with T_a (>100°C) up to the highest annealing temperature. This $H_\perp$ increase could be related to the structural changes occurring in the fibrils as will be discussed later.

4.2.2. Influence of annealing time

From Fig. 4 one observes a tendency of $H_\perp$ to increase with increasing annealing time. The hardness increase with t_a for 50°C $< T_a <$ 80°C could be related to a densification of the amorphous phase and/or an increase in the number or perfection of the smectic domains. For samples in which the triclinic structure is apparent ($T_a >$ 80°C), the higher $H_\perp$ values observed at long annealing times could be also related to an increase in crystallinity and crystalline lamellar thickness with t_a.

4.2.3. Elastic recovery

The rapid indentation anisotropy decrease for $T_a \sim 70$°C (Fig. 5) is connected with the concurrent decrease in the elastic properties of the fibrils which most probably relax with increasing annealing temperature. It was shown that after a change from nematic (20°C) to smectic (60°C), the precursor state appears at 70°C and the triclinic structure develops above 80°C). The indentation anisotropy decrease could be related to the development of the lamellar structure starting at about 70°C. One may imagine that in the amorphous layers, the local molecular orientation will be influenced by the relaxation mechanism occurring above T_g. As a result, the elastic recovery in the chain direction will decrease with increasing concentration of relaxed molecules in the amorphous layers. The observed decrease in the angle of a lamellar inclination (ϕ) as T_a increases is in accordance with the suggested relaxation of the molecules in the amorphous layers. In spite of this, it is interesting to note that rest of the mechanical anisotropy still remains preserved up to temperatures near the melting point.

4.2.4. Influence of the crystallinity

Hardness is known to vary with α_c following Eq. (4). The α_c values are derived from Eq. (1), continuously increase with T_a analogously to the ρ variation with T_a shown in Fig. 3. However, for $T_a <$ 100°C, the α_c increase is mainly because of the densification of smectic domains. Hence, the $H_\perp$ increase up to $T_a = 100$°C in Fig. 4 is mainly because of an increase in ρ rather than to the occurrence of X-ray crystallinity. Previous studies on isotropic semicrystalline PE had shown that H conspicuously varies with the macroscopic density [23,24]. The $H_\perp$ variation with T_a for $T_a \geq$ 100°C could be partly because of the α_c-increase with increasing annealing temperature (see Eq. (4)). Additionally, the microstructural changes occurring when raising the annealing temperature also contribute to a $H_\perp$ increase (given later).

4.2.5. Hardness-microstructure correlation

According to Eq. (4), the hardness should linearly increase with α_c. However, H_c is known to vary with l_c according to Eq. (5). We have seen that the crystallinity and crystal thickness increase with T_a (Table 1). In order to evaluate the independent influence of α_c and l_c on hardness, we have represented in Fig. 10 the variation of $H_\perp$ vs.

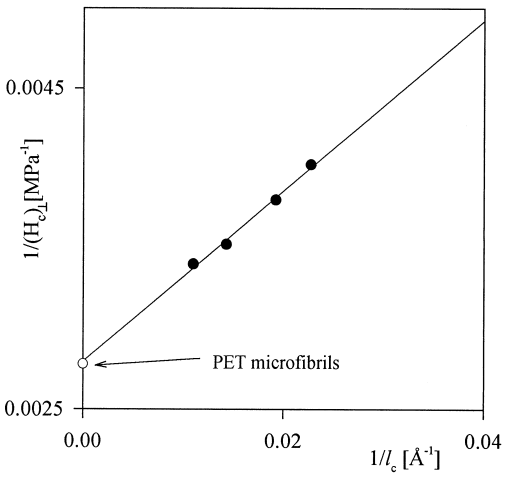

Fig. 11. Plot of $(H_c)_\perp^{-1}$ as a function of l_c^{-1}. Open circle: $H_\perp$ of highly crystalline chain-extended PET microfibrils.

α_c. The $H_\perp$ values for $T_a < 100°C$ were included and the corresponding α_c-values should be interpreted as discussed earlier. Eq. (4) could now be rewritten as:

$$H_\perp = \alpha((H_c)_\perp - (H_a)_\perp) + (H_a)_\perp. \quad (11)$$

Each $H_\perp$ value (for $T_a \geq 100°C$) in Fig. 10 fits to a straight line with slope $(H_c)_\perp - (H_a)_\perp$ and intercept $(H_a)_\perp$. If $(H_a)_\perp$ is known, then $(H_c)_\perp$ can be derived for each sample and subsequently related to the corresponding l_c value. If we approximate the $(H_a)_\perp$ value to the hardness of the cold-drawn sample ($\alpha_c = 0$, $(H_a^{glass})_\perp = 75$ MPa), then one would obtain a $(H_c)_\perp$ value (independent of l_c) of about 325 MPa for the samples annealed at $T_a \geq 140°C$ ($\alpha_c \geq 0.35$). Indentation experiments on PET microfibrils, which show a very high degree of crystallinity ($\alpha_c \sim 1$) and nearly extended chains ($l_c \rightarrow \infty$), give an $H_\perp$ value of 360 MPa [25]. Thus, not only the obtained value of $(H_c)_\perp^\infty \backsim 325$ MPa seems rather low but makes it also difficult to explain why our $(H_c)_\perp$ values do not vary with increasing l_c. This result suggests that the hardness of the amorphous constrained regions within the crystals should be higher than that of a completely amorphous oriented sample. However, the upper limit to the $(H_a)_\perp$ value is 140 MPa, which is the hardness of the sample annealed at $T_a = 100°C$ ($\alpha_c = 0.22$), where the smectic domains have completely disappeared (see Fig. 1f). If we assume a value of $(H_a)_\perp = 140$ MPa, we may draw a family of straight lines (see Eq. (11)), which are included in Fig. 10. Extrapolation of Eq. (11) at $\alpha_c = 1$ gives the crystal hardness $(H_c)_\perp$ for each l_c value. The same procedure could be applied for $(H_a)_\perp$ values in the range 75–140 MPa. Section 4.2.6 discusses the most reasonable $(H_a)_\perp$ values for the amorphous constrained phase based on the analysis of the $(H_c)_\perp$ vs. l_c data.

4.2.6. Hardness of infinitely thick crystals

According to Eq. (5), a plot of $1/(H_c)_\perp$ values versus $1/l_c$ values will fit into a straight line (if b is constant) of slope $b/(H_c^\infty)_\perp$ and ordinate intercept $1/(H_c^\infty)_\perp$. Fig. 11 illustrates the variation of $1/(H_c)_\perp$ with $1/l_c$ for samples annealed at $T_a \geq 180°C$ ($\alpha_c \geq 0.5$). In the derivation of the $(H_c)_\perp$ values, a value of $(H_a)_\perp = 140$ MPa was used. The data in Fig. 11 fit to a straight line. The intercept gives $(H_c^\infty)_\perp = 358$ MPa, which is in excellent agreement with $H_\perp$ of highly crystalline chain-extended PET microfibrils (=360 MPa) [25]. Lower $(H_a)_\perp$ values would yield higher intercepts and hence, smaller $(H_c^\infty)_\perp$ values. The earlier analysis suggests that the hardness value for the amorphous constrained regions ($(H_a)_\perp \sim 140$ MPa) is higher than that of the starting oriented amorphous material.

5. Conclusions

1. The sharp reflection on the meridian corresponding to a period of 10.7 Å, induced after annealing cold-drawn PET at 60°C, was associated with the occurrence of a smectic structure.
2. The SAXS maxima observed at 70°C indicate that a density fluctuation of 110 Å appears as a precursor before triclinic crystallization. From the SAXS pattern it is inferred that the layer structure is initially inclined about 62° from the draw direction.
3. Triclinic crystallization starts above 80°C, where the (010) planes are inclined by 10° from the draw direction.
4. The crystallization mechanism from the smectic structure, via the precursor state, into the final triclinic crystal is explained by a tilting mechanism. The molecular tilt and the inclination of the lamellar surface produce a density difference between regions in the precursor state. The triclinic crystals develop by a further tilt of 10°.
5. The hardness measurement of annealed oriented PET films permits to distinguish between: (a) amorphous oriented samples, (b) the smectic phase and (c) the crystalline fibrils.
6. Indentation anisotropy (related to elastic recovery) conspicuously decreases above $T_a \sim 70°C$ (i.e., near T_g). This was ascribed to a relaxation mechanism of the molecules in the amorphous layers in the chain direction.
7. Results suggest that the hardness value of the amorphous constrained regions within the semicrystalline fibrils is higher than that of the starting amorphous oriented material.

Acknowledgements

Grateful acknowledgement is due to the Dirección General de Investigación Científica y Técnica (DGICYT), Spain, for support of this investigation (Grant PB94-0049). A part of this work was performed under approval of the Photon Factory Advisory Committee (Proposal No. 97G-248).

References

[1] Keller A, Lester GR, Morgan LB, Hartley FD, Lord EW. Phil Trans R Soc 1954;A-1 247:13.
[2] Zachmann HG, Stuart HA. Makromol Chem 1960;41:131.
[3] Elsner G, Koch MHJ, Bordas J, Zachmann HG. Makromol Chem 1981;181:1263.
[4] Elsner G, Rickel C, Zachmann HG. Adv Polym Sci 1985;67:1.
[5] Gūnter B, Zachmann HG. Polymer 1983;24:1008.
[6] Asano T, Zdeick-Pickuth A, Zachmann HG. J Mater Sci 1989;24:1967.
[7] Bonart R. Kolloid-Z 1966;213:1.
[8] Yeh GSY, Geil PHJ. Macromol Sci B 1967;1:235.
[9] Yeh GSY, Geil PHJ. Macromol Sci B 1967;1:251.
[10] Daubeny Rde P, Bunn CW, Brown CJ. Proc Roy Soc 1954;A 226:531.
[11] Asano T, Seto T. Polym J 1973;5:72.
[12] Baltá Calleja FJ. Adv Polym Sci 1985;66:117.
[13] Baltá Calleja FJ. Trends Polym Sci 1994;2:419.
[14] Baltá Calleja FJ, Fakirov S. Trends Polym Sci 1997;5:246.
[15] Santa Cruz C, Baltá Calleja FJ, Zachmann HG, Stribeck N, Asano T. J Polym Sci Polym Phys B 1991;29:819.
[16] Baltá Calleja FJ, Baranowska J, Rueda DR, Bayer RK. J Mater Sci 1993;28:6074.
[17] Baltá Calleja FJ, Santa Cruz C, Asano TJ. Polym Sci Polym Phys B 1993;31:557.
[18] Baltá Calleja FJ, Öhm O, Bayer RK. Polymer 1994;35:4775.
[19] Rueda DR, Kubera L, Baltá Calleja FJ, Bayer RK. J Mater Sci Lett 1993;12:1140.
[20] Hatta I, Takahashi H, Matuoka S, Amemiya Y. Therm Acta 1995;253:149.
[21] Baltá Calleja FJ, Rueda DR, Porter RS, Mead WT. J Mater Sci 1980;15:765.
[22] Rueda DR, Baltá Calleja FJ, García Peña J, Ward IM, Richardson A. J Mater Sci 1984;19:2615.
[23] Baltá Calleja FJ, Martínez Salazar J, Cackovic H, Loboda-Cackovic J. J Mater Sci 1981;16:739.
[24] Martínez Salazar J, Baltá Calleja FJ. J Mater Sci 1983;18:1077.
[25] Krumova M, Fakinov S, Baltá Calleja FJ, Evstatiev M. J Mater Sci 1998;33.